Appl Phys B (2011) 105:239–244
DOI 10.1007/s00340-011-4686-x

Applied Physics B
Lasers and Optics

A narrowband optical parametric oscillator tunable over 6.8 THz through degeneracy with a transversely-chirped volume Bragg grating

N. Thilmann · B. Jacobsson · C. Canalias · V. Pasiskevicius · F. Laurell

Received: 14 January 2011 / Revised version: 9 June 2011 / Published online: 23 August 2011

Abstract An efficient nanosecond optical parametric oscillator (OPO) with output energies of 0.75 mJ using a periodically poled $KTiOPO_4$ crystal pumped at 532 nm and generating narrowband output continuously tunable over the range of 6.8 THz, between 1053 nm and 1075 nm, is demonstrated by employing a transversely-chirped volume Bragg grating. The tunable reflectivity spectrum of the chirped volume Bragg grating allowed a smooth transition between singly-resonant and doubly-resonant operation of the OPO without cavity rearrangement. This gave a unique possibility to experimentally verify theoretical predictions regarding the efficiency of type-I and type-0 phase matched degenerate OPOs pumped by multimode Q-switched lasers.

1 Introduction

Coherent sources producing narrowband radiation at two wavelengths simultaneously with easily tunable wavelength separation from zero to several THz while maintaining perfect pair-wise correlation between the photons at the two wavelength are of interest for THz generation by difference frequency mixing, coherent antistokes Raman scattering spectroscopy, cascaded pumping of mid-infrared optical parametric frequency converters [1–3], and other applications. Optical parametric oscillators operating close to degeneracy seemingly have the characteristics satisfying the requirements above. By employing type-II phase matching one can obtain narrow bandwidth signal and idler output close to and at degeneracy, at the expense of low tuning flexibility and lower parametric gain due to substantially lower nondiagonal $\chi^{(2)}$ tensor components in ferroelectric nonlinear materials such as $KTiOPO_4$, $LiNbO_3$, and $LiTaO_3$. The use of these materials brings the substantial advantage of the possibility to engineer quasi-phase matched (QPM) nonlinear interactions that are free of Poynting vector walk-off. The highest efficiency of the QPM nonlinear interaction is achieved in above-mentioned materials for type-0 phase matching where all the interacting waves are polarized parallel to the polar axis, i.e., employing the d_{33} nonlinear coefficients. Sometimes this interaction, although efficient, can be considered undesirable because the almost equal signal and idler group velocities close to degeneracy result in a very broad parametric gain bandwidth [2, 4, 5]. On the other hand, the broad parametric gain bandwidth at degeneracy can be utilized to simplify wide tuning of the signal and idler frequency separation without involving a non-colinear interaction geometry associated with beam steering effects [6].

In this work, we used a type-0 QPM OPO employing periodically poled $KTiOPO_4$ (PPKTP) as the gain medium to demonstrate tunability of the signal and idler separation over more than 6 THz around the degeneracy wavelength of 1064 nm. The tuning arrangement takes advantage of the spatially varying reflectivity spectrum of a transversely-chirped volume Bragg grating (TC-VBG) and allows for rapid OPO tuning by a simple linear translation of the TC-VBG. Reflective volume Bragg gratings (VBGs) written in photo-thermo-refractive glass [7] fulfill the demands for spectral selection in pulsed OPOs, providing narrow bandwidth and—if required—high reflectivity, low loss in the near-infrared, as well as high durability and damage threshold [8]. Tunable coherent light can be achieved by rotating the VBG [8, 9] or alternatively by transversal translation of

N. Thilmann (✉) · B. Jacobsson · C. Canalias · V. Pasiskevicius · F. Laurell
Department of Applied Physics, Royal Institute of Technology, 10691 Stockholm, Sweden
e-mail: nt@laserphysics.kth.se

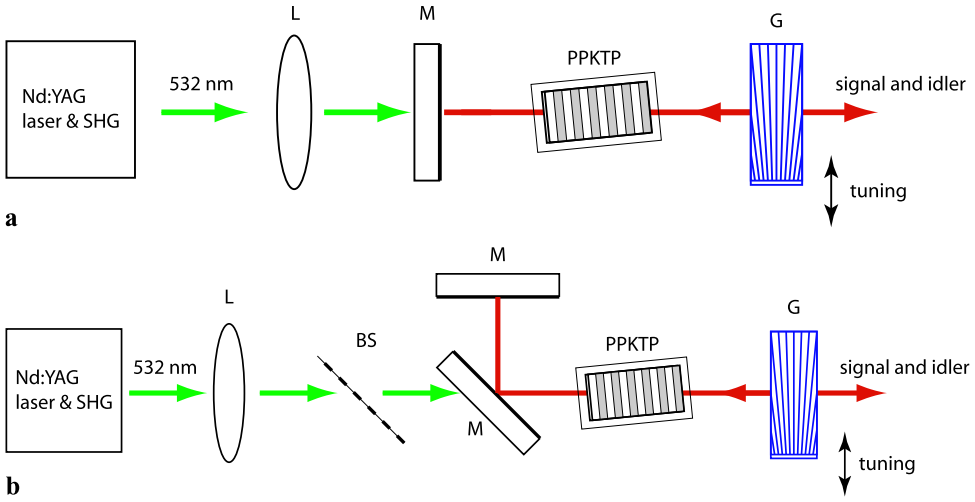

Fig. 1 The OPO setup in the linear configuration (**a**) and in the L-configuration (**b**) *L*: focusing lens; *M*: mirror with high reflectivity for signal and idler; *G*: transversely-chirped volume Bragg grating; BS: beam sampler

the TC-VBG [10]. This tuning capability was demonstrated for a nondegenerate singly-resonant OPO. In this work, our goal was to attain tunability of the signal-idler separation from zero to several THz as required by the applications above. In the process, the use of a TC-VBG enables smooth transition from doubly-resonant to singly-resonant OPO operation without rearranging the cavity and, therefore, comprises a unique setup for investigating both regimes of operation. This is important in the context of the recently observed cavity length resonances in singly-resonant and doubly resonant OPOs [11, 12], as well as for the efficiency dependence of doubly resonant OPOs on the coherence properties of the pump [5].

2 Experiments and discussion

The linear tunable OPO cavity used in this work is shown in Fig. 1(a). A 10 mm-long PPKTP crystal with a QPM periodicity of 9.01 μm was used as the gain medium. This periodicity corresponds to degenerate parametric gain at 1064 nm for a type-0 QPM interaction. The crystal was pumped at 532 nm by a frequency-doubled Q-switched Nd:YAG laser delivering 6 ns-long pulses at a repetition rate of 20 Hz and a max output energy of 6 mJ. The pump beam was focused by a 200 mm focal length lens into the PPKTP crystal, providing a beam waist of 220 μm radius (intensity $1/e^2$). A half-wave plate in combination with a polarizer allowed to control of the pump energy launched into the OPO. The OPO cavity was completed by a dielectric mirror as the input coupler, and a TC-VBG as the output coupler. Tuning was achieved by lateral translation of the TC-VBG output coupler. The physical length of the cavity was 20 mm. The PPKTP crystal was placed on a temperature-controlled copper block and stabilized at 25°C. The crystal was tilted by about 5° to the resonator axis to prevent parasitic oscillations on the crystal surfaces. For the same reason, both the crystal and the grating were anti-reflection coated for all interacting wavelengths and the grating's glass surfaces were wedged with regard to the grating planes. For direct characterization of the back-converted power the setup shown in Fig. 1(b) was employed. In this setup, the OPO was pumped through a turning mirror, highly reflective around 1064 nm and with high transmission at the sum-frequency of the signal and the idler. In this setup, a glass-plate pickup was inserted into the pump beam to capture the backwards propagating back-converted light.

The reflectivity spectrum of the volume Bragg grating was characterized by directing a cw Ti:Sapphire laser beam onto it and tuning the wavelength of the laser between 1054–1067 nm while measuring the transmitted and reflected power. The measurement was repeated for several positions of the grating. The spot size of the Ti-sapphire laser was about 220 μm (radius $1/e^2$) which corresponds to the spot size in the OPO experiments described below. The measured spatial distribution of the TC-VBG reflectivity is shown in Fig. 5 (red triangles). The peak reflectivity of the VBG varied between 50–75% at wavelengths from 1052 nm to 1064 nm and dropped to just below 20% at 1066 nm. The chirp of the 17 mm wide grating was linear and found to be 0.8 nm/mm. The measured reflectivity bandwidth (FWHM) ranged from 0.4 nm to 0.6 nm and was only slightly influenced by the chirp of the grating due to the small spot size on the grating during the experiments.

The resonating wavelength of the OPO, i.e., the signal or the idler wavelength, was easily locked by the TC-VBG. The measured energy characteristics for the singly-resonant OPO locked off-degeneracy at 1059 nm signal (where the TC-VBG reflectivity is 69%) are shown in Fig. 2. The OPO pump threshold was reached at a pump energy of 0.2 mJ, corresponding to the peak intensity of 22 MW/cm^2. At pump energies 10-times above the threshold, the total IR

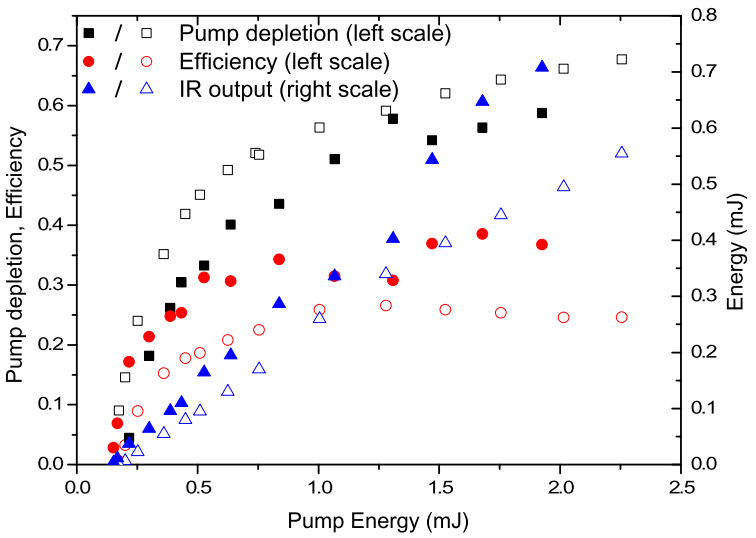

Fig. 2 Pump depletion (*squares*), efficiency (*circles*), and output energy (*triangles*) of the OPO measured at a signal wavelength of 1059 nm and 1064 nm (*solid and open symbols*, respectively)

output energy reached 0.8 mJ. The depletion was found to be 60% at this pump energy while the total conversion efficiency reached 40% for the same input energy. The difference between depletion and efficiency can be explained by losses at the signal wavelength caused by scattering in the TC-VBG (few percent) and remnant reflectivity of the antireflection coatings on the crystal and TC-VBG surfaces.

Once aligned, the OPO could be tuned over the whole spectral range, from 1052 nm to 1066 nm, by simple lateral translation of the grating. Figure 3(a) shows the dependence of the signal and the idler wavelengths as functions of the OPO beam position on the TC-VBG. Figure 3(b) shows overlaid OPO spectra close to degeneracy. The spectra were measured using an optical spectrum analyzer (ANDO AQ-6315; resolution of 0.05 nm) synchronized with the pump laser. Figure 3 reveals that this particular TC-VBG allows straightforward tuning of the signal and idler frequency separation from zero to 6.8 THz while keeping an approximately constant spectral width of the OPO output. As the spectral width of the TC-VBG reflectivity is determined by the spatial chirp of the grating and by the beam size as the well as spatial chirp of the signal (pulse front tilt), then the spectral width of the OPO output is engineerable by an appropriate choice of these design parameters.

Two representative spectra, at degeneracy and off-degeneracy, produced by the OPO with the TC-VBG and operating six times above threshold are shown in Fig. 4 (solid and dashed lines, respectively). The resonating OPO wave had a spectral bandwidth of ~0.6 nm (160 GHz) off degeneracy and ~0.75 nm (200 GHz) at degeneracy. This corresponds well to the bandwidth of the TC-VBG for the given OPO beam diameter. In comparison, the spectrum depicted in Fig. 4 with dotted line was obtained using a broadband Fresnel reflection from an uncoated BK7 glass flat as the OPO output coupler. The FWHM bandwidth of 11 nm for this

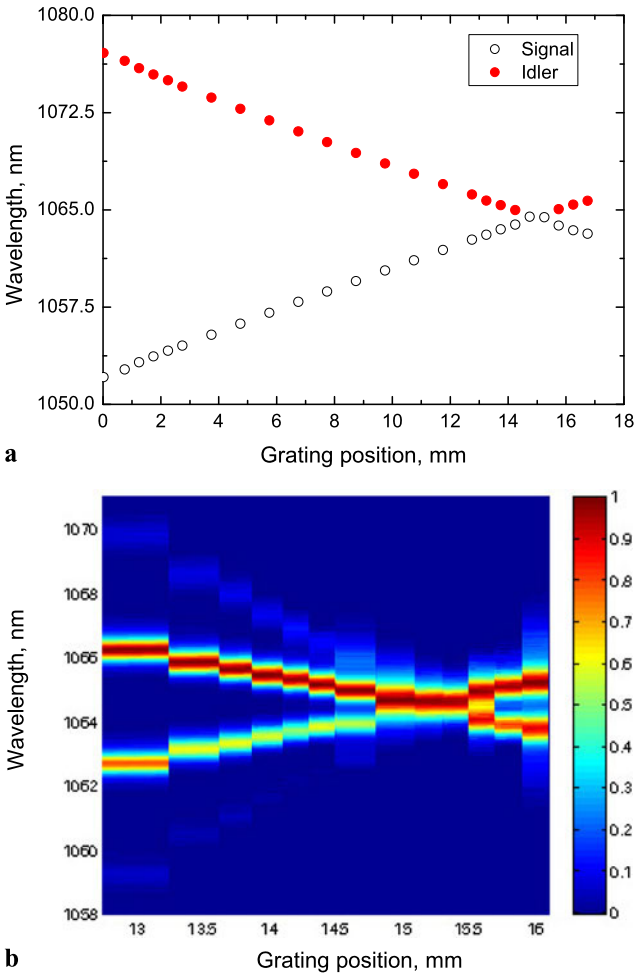

Fig. 3 Signal and idler wavelength versus the position of the transversely-chirped volume Bragg grating (**a**). Map of the normalized optical spectra for different grating positions near the OPO degeneracy (**b**)

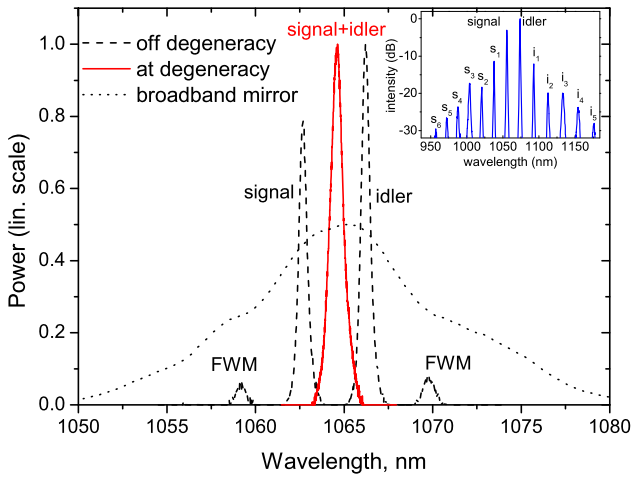

Fig. 4 Spectrum of OPO output at degeneracy (*solid line*), off degeneracy (*dashed line*) and with a broadband mirror as output coupler (*dotted line*). The insert shows a logarithmic spectrum off degeneracy

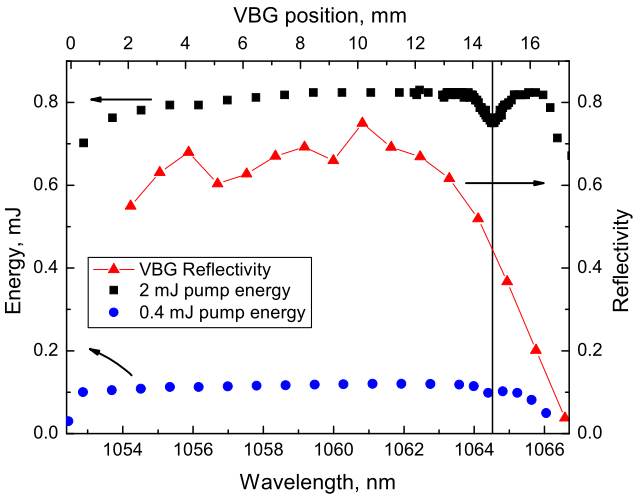

Fig. 5 Reflectivity of the transversely-chirped volume Bragg grating (*triangles*, *right scale*) and the total infrared output energy for pump energies of 2 mJ (*squares*, *left scale*) and 0.4 mJ (*filled circles*, *left scale*) versus grating position and the equivalent resonant wavelength

low finesse cavity OPO reveals the available parametric gain bandwidth from the PPKTP crystal. For the off-degeneracy OPO, in addition to the signal and idler peaks, smaller peaks can also be seen in the output spectrum (insert in Fig. 5). These spectral peaks are the result of a cascaded $\chi^{(2)}$:$\chi^{(2)}$ four-wave mixing (FWM) process [13, 14]. The equidistant frequency comb as seen in the inset of Fig. 4 (note the logarithmic scale) has additional spectral peaks with the frequency separation of $\delta = \omega_s - \omega_i$, and are produced by cascades of the processes $\omega_{s1} = \omega_s + \omega_s - \omega_i$ and $\omega_{i1} = \omega_i + \omega_i - \omega_s$. Here, the $\omega_s, \omega_i, \omega_{s1}, \omega_{i1}$ denote the signal, the idler, the first high-frequency sideband and the first low-frequency sideband, respectively. Eventually, the spectral extent of the cascade is determined by the phase mismatch of the sum-frequency processes $\Delta k_1 = 2k_s - k_i - K_{\mathrm{QPM}}$, $\Delta k_2 = 2k_i - ks - K_{\mathrm{QPM}}$ ($k_s, k_i, K_{\mathrm{QPM}} = 2\pi/\Lambda$ are the signal, the idler wave vectors and the wave vector of the QPM grating with periodicity Λ, respectively) and the available parametric gain bandwidth. Obviously the frequency separation of the FWM comb is tuned when TC-VBG is translated, as can be seen in the Fig. 3(b). This property can be useful for some applications considering that the sideband amplitudes can be equalized by using an additional optical parametric amplification stage with appropriately shaped parametric gain. This can easily be achieved using a properly designed QPM parametric gain structure. For the TC-VBG OPO operating off degeneracy, the power in the FWM sidebands did not exceed 10% of the total generated near-infrared power.

The OPO output energy varies only slightly as the wavelength of the resonant signal is varied between 1053 nm and 1066 nm as can be seen in Fig. 5. The slight decrease in the output energy obtained as the OPO resonant wave is tuned toward shorter wavelengths is determined primarily by the decrease in parametric gain (cf. Fig. 4). At the longer wavelength side, the output is limited by the reflectivity range of TC-VBG. An interesting feature in Fig. 5 is the dip in the OPO output energy at degeneracy, while the IR output energy is fairly constant over the rest of the tuning range. The dip is about 0.07 mJ (8%) deep and 0.6 nm wide (FWHM) for a pump energy of 2 mJ. Moreover, the decrease in OPO efficiency at and close to degeneracy was systematic, i.e. occurring at all pump powers. The spectral width of the dip corresponds to the spectral bandwidth of the TC-VBG and therefore is related to the transition from singly resonant to doubly resonant oscillation. Although the decrease in OPO efficiency in the doubly resonant regime is relatively small, we believe that this feature infers an important physical mechanism as outlined below.

The decrease of the OPO output cannot be explained by the variation of the reflectivity of TC-VBG as the OPO output recovers once the OPO is tuned to longer wavelengths beyond degeneracy where the reflectivity of the TC-VBG decreases further. This can be understood by taking the high gain provided by the OPO into account. As seen in Fig. 2, the OPO thresholds are equal for different operating wavelengths, i.e., close to and at degeneracy. This confirms that the decrease of the OPO output cannot be explained by a difference in the outcoupling. However, in principle the decrease in the OPO output can be caused by an increase of the loss due to back-conversion. To quantify this, we examined the amount of backward back-conversion obtained by changing the cavity to an L-cavity configuration (cf. Fig. 1(b)). At degeneracy, we measured no more than 0.01 mJ of light back-converted to the pump wavelength at the maximum pump energy of 2 mJ. Off-degeneracy, no back-conversion could be observed. Thus, the maximum

back-conversion can only account for about 30% of the observed decrease in the OPO efficiency at 2 mJ pump energy. In fact, this discrepancy becomes even larger for lower pump energies. Instead, we believe the observed efficiency dip at degeneracy can be explained by taking into account the mutual coherence of the OPO radiation circulating in the cavity and the pump. This would be the first direct experimental demonstration of the physical mechanism first proposed theoretically in [5].

The field envelopes of the pump, the signal and the idler A_p, A_s, A_i are related by the usual coupled-wave equations for broadband plane waves propagating along the z-direction:

$$\begin{aligned}\left(\partial_z + v_{\mathrm{gs}}^{-1}\partial_t\right)A_s &= i\sigma_s A_p A_i^* \\ \left(\partial_z + v_{\mathrm{gi}}^{-1}\partial_t\right)A_i &= i\sigma_i A_p A_s^* \\ \left(\partial_z + v_{\mathrm{gp}}^{-1}\partial_t\right)A_p &= i\sigma_p A_s A_i\end{aligned} \tag{1}$$

where v_{gj}, σ_j $(j = p, s, i)$ are the corresponding group velocities and coupling coefficients while ∂_z and ∂_t denote partial derivatives over propagation direction and time. By considering the coordinate frame moving with the group velocity of the pump and, for simplicity, disregarding pump depletion, the equations for the signal and idler can, after introduction of a new variable $\zeta = t - z/v_{\mathrm{gp}}$, be rewritten as:

$$\begin{aligned}\delta_{sp}\partial_\zeta A_s &= i\sigma_s A_p A_i^* \\ \delta_{ip}\partial_\zeta A_i &= i\sigma_i A_p A_s^*\end{aligned} \tag{2}$$

where $\delta_{sp} = v_{\mathrm{gs}}^{-1} - v_{\mathrm{gp}}^{-1}$, $\delta_{\mathrm{ip}} = v_{\mathrm{gi}}^{-1} - v_{\mathrm{gp}}^{-1}$ are the group-velocity mismatch between signal and pump and idler and pump, respectively. It is instructive to recast (2) into an integral equation by formally integrating the second equation of (2), taking its complex conjugate, and inserting it into the first equation with subsequent formal integration. This procedure results in the following equation:

$$A_s(\zeta'') = \frac{\sigma_s^2}{\delta_{\mathrm{sp}}^2}\int_{-\infty}^{\zeta''}\int_{-\infty}^{\zeta'} A_p(\zeta)A_p^*(\zeta')A_s(\zeta)\,d\zeta\,d\zeta', \tag{3}$$

where it was taken into account that at degeneracy the group velocities and the coupling coefficients of the signal and the idler are approximately equal. From this equation, one can see that the generated signal amplitude in the parametric process at different moments in time will depend on the pump correlation and the previous signal amplitude. The correlation time of the pump laser used in our experiments was estimated to be 140 ps from the threshold of a two-beam pumped OPO [13]. Considering that the round-trip time in the doubly resonant OPO is 197 ps, and assuming a Gaussian dependence of the pump correlation function, would result in a probability of 0.13 that the signal and the idler fields for each subsequent round-trip in the doubly resonant OPO regime would encounter the correct phase of the pump field for coherent amplification. Due to the fact that the doubly resonant OPO is over-constrained, the average gain is partly suppressed, i.e., in subsequent round-trips the signal and/or the idler phase might not match the pump phase while at the same time being over constrained and, therefore, a lower output energy is observed in this case. On the other hand, in a singly-resonant OPO, where the idler is not resonated and can hence take any phase value dictated by the relation, $\varphi_p - \varphi_s - \varphi_i = \pi/2$, the parametric gain will not depend on the relative coherence of the pump and the signal and, therefore, allows the higher output energy—in our case outside the degenerate region.

3 Conclusions

We have demonstrated a narrowband tunable OPO with a transversely-chirped volume Bragg grating as the output coupler. The OPO was pumped with 6 ns pulses at 532 nm and operated at and close to degeneracy. The ~0.6 nm bandwidth output could be tuned from 1053 nm to 1075 nm by translating the TC-VBG. The use of this configuration offered a unique possibility to investigate multimode-pumped singly-resonant and doubly-resonant operation regimes without changing the cavity configuration. In particular, when operating exactly at degeneracy, the OPO generated a single spectral peak with 0.75 nm bandwidth and 0.75 mJ of energy. It was determined that the OPO efficiency in the doubly resonant OPO is somewhat lower than in the singly resonant regime due to the limited coherence of the pump, in accordance to the theoretical expectations in [5]. However, the efficiency decrease was only 7% for the TC-VBG locked degenerate OPO operating at pump intensities ten times above threshold. Considering that the same parameters of operation can be transferred to a VBG-locked OPO pumped at 1064 nm and operating at degeneracy, the multimode pumping becomes an interesting option, simplifying cascaded OPO schemes used for mid-infrared generation [1, 2, 15].

Acknowledgements We acknowledge Optigrate for providing the transversely-chirped volume Bragg grating used in this work. The Swedish Research Council, Linneus Centre ADOPT, and the K.A. Wallenberg Foundation partially funded this research. We also received funding from the European Community's Seventh Framework Program FP7/2007-2011 under Grant No. 224042.

References

1. M.W. Haakestad, G. Arisholm, E. Lippert, S. Nicolas, G. Rustad, K. Stenersen, Proc. SPIE **6998**, 12 (2008)
2. M. Henriksson, M. Tiihonen, V. Pasiskevicius, F. Laurell, Opt. Lett. **31**, 2006 (1878)

3. K.L. Vodopyanov, O. Levi, P.S. Kuo, T.J. Pinguet, J.S. Harris, M.M. Fejer, B. Gerard, L. Becouarn, E. Lallier, Opt. Lett. **29**, 1912 (2004)
4. G. Kalmani, A. Arie, P. Blau, S.Sh. Pearl, A.V. Smith, Opt. Lett. **30**, 2146 (2005)
5. A.V. Smith, D.J. Armstrong, M.C. Phillips, R.J. Gehr, G. Arisholm, J. Opt. Soc. Am. B **20**, 2319 (2003)
6. M. Tiihonen, V. Pasiskevicius, F. Laurell, Opt. Express **12**, 5526 (2004)
7. O. Efimov, L. Glebov, L. Glebova, K. Richardson, V. Smirnov, Appl. Opt. **38**, 619 (1999)
8. B. Jacobsson, M. Tiihonen, V. Pasiskevicius, F. Laurell, Opt. Lett. **30**, 2281 (2005)
9. B. Jacobsson, C. Canalias, V. Pasiskevicius, F. Laurell, Opt. Lett. **32**, 3278 (2007)
10. B. Jacobsson, V. Pasiskevicius, F. Laurell, E. Rotari, V. Smirnov, L. Glebov, Opt. Lett. **34**, 449 (2009)
11. G. Arisholm, E. Lippert, G. Rustad, K. Stenersen, Opt. Lett. **25**, 1654 (2000)
12. M. Henriksson, L. Sjoqvist, V. Pasiskevicius, F. Laurell, Opt. Express **18**, 10742 (2010)
13. M. Tiihonen, V. Pasiskevicius, Opt. Lett. **31**, 3324 (2006)
14. X. Zhang, H. Giessen, Appl. Phys. B, Lasers Opt. **79**, 441 (2004)
15. M. Henriksson, L. Sjöqvist, V. Pasiskevicius, F. Laurell, Opt. Express **17**, 17582 (2009)